sustainability

MDPI

Article

An Alternative Carbon Source from Cassava Residue Saccharification Liquid for In-Situ Fabrication of Polysaccharide Macromolecule/Bacterial Cellulose Composite Hydrogel: A Comparative Study

Li Ji, Wenwen Xue, Liwei Zhu and Jianxin Jiang *

Department of Chemistry and Chemical Engineering, MOE Engineering Research Center of Forestry Biomass Materials and Bioenergy, National Forest and Grass Administration Woody Spices (East China) Engineering Technology Research Center, Beijing Forestry University, Beijing 100083, China
* Correspondence: jiangjx2004@hotmail.com; Tel.: +86-10-6233-8267

Abstract: Bacterial cellulose (BC) is a biopolymer with vast application prospects, and its production demands culture media rich in carbon sources. Here, we researched a modified in situ strategy for preparing composite hydrogels comprising BC and sodium alginate (SA) or sodium hyaluronate (SH), termed as SA-BC and SH-BC, respectively. A new carbon source for BC generation was successfully developed from cassava residue saccharification liquid (CSL), in an attempt to better exploit the residue and decrease the costs of BC production. SA or SH was mechanically hydrogen-bonded with BC nanofibers to form porous nanostructures. Compared to the native BC, the mechanical strength of SH-BC with 1% SH was 61% higher and the thermal stability was also improved. A considerable difference in the cumulative drug-release rate of 93% in 66 h revealed that SA-BC with 0.5% SA exhibited a higher pH sensitivity due to its abundant fibrous layers, the -COO^--electrostatic repulsion, and the weakened hydrogen-bonding at pH 7.4. Such in situ-derived composite hydrogels could provide insights for BC functionalization and advance understanding of polysaccharides' conversion to biomaterials with favorable biocompatibility and sustainability.

Keywords: in situ biosynthesis; bacterial cellulose; cassava residue saccharification liquid; polysaccharides; drug delivery pH sensitivity

check for updates

Citation: Ji, L.; Xue, W.; Zhu, L.; Jiang, J. An Alternative Carbon Source from Cassava Residue Saccharification Liquid for In-Situ Fabrication of Polysaccharide Macromolecule/Bacterial Cellulose Composite Hydrogel: A Comparative Study. *Sustainability* **2022**, *14*, 14277. https://doi.org/10.3390/su142114277

Academic Editor: Peng Zhang

Received: 6 October 2022
Accepted: 30 October 2022
Published: 1 November 2022

Publisher's Note: MDPI stays neutral with regard to jurisdictional claims in published maps and institutional affiliations.

Copyright: © 2022 by the authors. Licensee MDPI, Basel, Switzerland. This article is an open access article distributed under the terms and conditions of the Creative Commons Attribution (CC BY) license (https://creativecommons.org/licenses/by/4.0/).

1. Introduction

Polysaccharides could provide microbial strains (e.g., *Acetobacter xylinum*, AX) of medium carbon sources (i.e., glucose) for BC generation [1]. The conversion of sugar monomers to energy and chemicals as end products is considered to be a "sugar platform" [2]. Glucose is a major component of the lignocellulosic biomass and is regarded as the main source for valuables production (e.g., bioethanol, biodiesel, xylo-oligosaccharide) [3]. However, the high cost, facility corrosion, and ecological environmental pollution associated with these production processes are drawbacks that cannot be neglected. Based on the "green chemistry" concept, new developmental strategies are necessary to establish a lignocellulose-to-materials value chain with a competitive advantage [4]. The solid waste of the cassava starch industry, termed cassava residue (CR), is a typical lignocellulosic polysaccharide material rich in cellulose (30 ± 10%) and starch (40 ± 10%) [5]. CR is based on the inedible parts of plants, which would not affect the food supply. In economic terms, the relatively fast growth process of lignocellulosic biomass, to a certain extent, reduces costs compared with using commercial glucose as the carbon source being exploited by AX for the in situ preparation. In addition, the well-executed fermentation processes of sugar and starch biorefineries have been considered excellent bases for expanding the studies on cellulose and starch saccharification [6]. Therefore, exploring the potential of the

saccharified cellulose and starch liquid of CR as a carbon source for the AX fermentation medium in replacement for glucose is advantageous.

A multifunctional BC-based hydrogel is a novel and natural polymer for research and applications [1,7–9]. Considering their excellent properties, especially satisfactory biocompatibility, BC hydrogels have been widely employed in biomedicine for oral cavity protection, medical cosmetology, and drug delivery [10–12]. However, their utilization remains unsatisfactory, owing to the lack of specific characteristics, especially in pharmaceutical applications requiring intelligent-swelling performance, cell penetration ability, and defined mechanical properties [6]. Consequently, modifications such as adding a pore-forming agent to induce a macroporous structure [13] and utilizing electron-beam radiation to initiate crosslinking and enhance mechanical strength [14] have been performed. However, these modification strategies involve severe challenges. It would be difficult to remove the harmful chemical initiators; the modified BC hydrogel structure could be damaged by the repeated removal of residual chemicals, and the strong reagents and complicated chemical polymerization scheme render control of the entire process during fabrication difficult.

Due to the unique 3D network and hydroxyl-rich groups of BC, a variety of macromolecules can be embedded in its self-assembly matrix through an in situ biosynthesis process that lacks severe conditions [15]. The additional hydrogen bonds created between the cellulose microfibrils and the macromolecular additives help to produce a modified 3D cellulose network with an effective nanoparticle dispersion rate. Therefore, the yield, structure, and properties of BC can be adjusted and improved [16] to create effective, in situ modifications [17,18]. A recent study demonstrated that the in situ BC, modified by xylan and xyloglucan added to the culture media, exhibited better thermal stability and tensile properties [19]. In another study, potato starch in the medium produced a nontoxic and biodegradable in situ composite BC hydrogel, demonstrating its in vivo implantation potential for tissue engineering [13]. Both sodium alginate (SA) and sodium hyaluronate (SH) are natural polysaccharides [9]. SA has been demonstrated to promote cell delivery in tissue engineering [20]. In previous studies, SH also displayed broad prospects for biomedicine in hydrogel systems [21]. However, although studies on BC modification are common, comparative studies of composite BC hydrogels with different macromolecules are limited.

Thus, SA or SH may favor the interaction of BC through hydrogen bonds induced by the in situ synthesis modification. The main goal of this work was to test the hypothesis that the in situ-fabricated BC-based hydrogel could be a promising candidate for biomedical application. As a glucose substitute, the influence of the saccharified CR cellulose and the use of the starch liquid as the carbon source in the AX fermentation medium was studied. The reaction products were characterized by scanning electron microscopy (SEM), Fourier-transform infrared (FTIR), thermogravimetric analysis (TGA), X-ray diffraction (XRD), swelling property, and tensile strength. Regarding the biocompatibility of the hydrogels, in vitro tests on Hela cells were carried out. Finally, the effectivity of SA and SH was compared by their preliminary in vitro drug-release behaviors, using bovine serum albumin (BSA) as the model protein, and the pH sensitiveness of the hydrogels and their potential as controlled drug-delivery vehicles were evaluated.

2. Materials and Methods

2.1. Preparation of the Native BC and the SA-BC/SH-BC Composite Hydrogels

The materials information is shown in the Supplementary Materials. The native BC was inoculated on Hestrin–Schramm (HS) medium (2.00% glucose, 0.50% yeast extract, 0.50% peptone, 0.27% disodium hydrogen phosphate, and 0.12% citric acid, pH 6.0 at 30 °C). The SA-BC/SH-BC composite hydrogels were also prepared by using HS medium, while CSL (5.00%, *w/w*) was used as the carbon source to completely replace glucose in the medium (5.00% CSL, 0.50% yeast extract, 0.50% peptone, 0.27% disodium hydrogen phosphate, and 0.12% citric acid, pH 6.0 at 30 °C). The detailed saccharification methods

of CR-starch and CR-cellulose are described in the Supplementary Materials. The above-mentioned medium was supplemented with SA and SH, respectively, at the moment of inoculation at the dosages of 0.25, 0.5, and 1.0% (Table S1, Supplementary Materials). According to the previous study, a supplement of SA in the culture medium was performed in the range of 0–1.0%, synthesizing the novel bacterial cellulose membrane. To avoid the inhibition of cell production, the maximum amount of SA was limited to 1.0% [22]. Therefore, SA was added to the medium at dosages of 0.25, 0.5, and 1.0% for efficient optimization of this in situ synthesization. SH also displayed broad prospects in hydrogel systems. For the purpose of a comparative study, the medium was supplemented with SH at the same dosage to evaluate the characterizations and properties of SA-BC and SH-BC composite hydrogels. The pH was adjusted to 6.0 with 0.5% NaOH solution [23]. After 10 days of static cultivation, the SA-BC and SH-BC composites were collected. They were boiled in 0.5% NaOH solution for 30 min and rinsed with distilled water repeatedly for the removal of the remaining medium and microorganisms. The freeze-dried samples (−80 °C, 24 h) were used for further characterization.

2.2. Mass Yield (MY) of Composite BC Hydrogels

The freshly, as-prepared composite BC hydrogels were removed from the beaker and freeze-dried to a constant weight. The MY percent of the hydrogels was calculated using Equation (1):

$$\mathrm{MY\%} = \frac{\mathrm{W_0} - \text{Mass of additive}}{\mathrm{W_g}} \times 100 \quad (1)$$

where $\mathrm{W_0}$ is the dried weight of the as-prepared hydrogel and $\mathrm{W_g}$ is the glucose weight in the HS medium.

2.3. The Glucose Concentration and the Colony-Forming Units (CFUs) Analysis during Microbial Synthesis

The consumption of glucose and the number of CFUs were evaluated according to the reported study during the cultivation stage [18]. A series of hydrogel samples were collected every day to determine the glucose concentration of the culture medium within 14 days. The concentration of glucose at each point of the time period was evaluated by HPLC (Waters 2695e) with the HPX-87H column. There were three replicates at each cultivated time point.

2.4. Structural Characterization

After 48 h of lyophilization, the freeze-dried hydrogel powders were used for FTIR analysis (Bruker Co., Berlin, Germany) and XRD analysis (Bruker Daltonics Inc., USA) to study the structural characterization of the SA-BC and SH-BC hydrogels. The surface appearances of the hydrogels were observed by SEM (Merlin, Carl Zeiss AG, Oberkochen, Germany) and the freeze-dried samples were cut into thin slices and sputtered with gold for 10 min. The TGA of the samples was measured using the Shimadzu TGA-50 (Shimadzu Scientific Instruments, Columbia, MD, USA) and all the measurements were performed under nitrogen at a flow rate of 20 mL/min and heated at 10 °C/min from 20 to 600 °C.

2.5. Tensile Properties

The composite BC hydrogels were cut to 20 × 5 mm with an average cross-sectional area of 10 $\mathrm{mm^2}$ for each tensile sample using a universal tensile-strength testing machine (Shanghai Xiang Jie Instrument Co., Ltd., Shanghai, China, XJ830D) equipped with a 100 N-load cell at an ambient temperature of 25 °C. The relative humidity was 50 ± 5%, which was measured using a psychrometer (Shanghai Yi Pin Instruments & Meters Co., Ltd., Shanghai, China, HM18). The water content of the hydrogel samples was measured by an electronic balance. The excess water on the sample surfaces was wiped with filter paper before the test and, afterward, the samples were put in the drying oven at 80 °C until they were a constant weight. According to the lost weight of the dried samples, we calculated

the water content. Consequently, the average water content of the native BC, SH-BC-0.25, SH-BC-0.5, SH-BC-1, SA-BC-0.25, SA-BC-0.5, and SA-BC-1 was 81.64 ± 0.32%, 81.37 ± 0.21%, 82.18 ± 0.17%, 82.06 ± 0.19%, 81.75 ± 0.11%, 81.93 ± 0.28%, and 82.10 ± 0.22%, respectively. The initial clamp distance was set as 10 mm and the speed was a constant value of 10 mm/min. Each group had three replicates [24].

2.6. Swelling Ratio (SR) Study

The purified composite BC hydrogels were freeze-dried to a constant weight. The hydrogels were immersed in distilled water for 24 h. The three parallel experiments of SR were measured over time intervals, after the excess water existing on the sample surfaces was blotted with filter paper. The SR percent was calculated by Equation (2):

$$SR\% = \frac{m_2 - m_1}{m_1} \times 100 \quad (2)$$

where m_1 is the dried weight and m_2 is the swollen weight.

2.7. Drug Loading Study

Simulated gastric fluid (SGF) was prepared by adding HCl to 2 g/L NaCl solution to adjust the pH value to 1.2. Simulated intestinal fluid (SIF) was prepared by adding 0.1 mol/L NaOH to 13.6 g/L KH_2PO_4 solution to adjust the pH value to 6.8 [25]. BSA was loaded as the drug model into the freeze-dried hydrogels using the swelling-diffusion method. The BSA solution of 1% (*w/v*) was prepared in SGF, SIF, and PBS at pH 1.2, 6.8, and 7.4, respectively. The freeze-dried hydrogels of a certain mass were immersed in the BSA solution (25 mL). After the incubation (37 °C, 2 days), the removed hydrogels were washed with SGF, SIF, and PBS. The amount of BSA left in the solution was detected at the wavelength of 280 nm with a UV spectrophotometer (UV-6100A; Shjingmi, Japan) [26]. The entrapment efficiency (EE) of the drug models in the hydrogels was calculated by Equation (3):

$$EE\% = \frac{W_1 - W_f}{W_1} \times 100 \quad (3)$$

where W_1 is the total mass of BSA before the drug loading, and W_f is the total mass of BSA remaining in the solution after drug loading.

2.8. In Vitro Drug Release Study

The in vitro drug release studies were conducted using the immersion method [26]. The hydrogel samples, loaded with the drug model, were immersed into 25 mL of SGF, SIF, and PBS, respectively, under the incubation conditions of 37 °C and 50 rpm until the maximum release. When the sample liquid of 0.5 mL was removed from the release culture medium at the predetermined time point, fresh medium of 0.5 mL was added. The concentrations of the drug models in the liquid samples were measured by a UV spectrophotometer at 280 nm. The results were calculated by the cumulative percentage release using Equation (4):

$$\text{Cumulative drug release}\% = \frac{W_t}{W_b} \times 100 \quad (4)$$

where W_t is the amount of the BSA released from the hydrogel at time t and W_b is the amount of the BSA loaded onto the hydrogel. The release study was performed in triplicate. The in vitro cell cytotoxicity using the MTT assay is detailed in the Supplementary Materials.

2.9. Zeta Potential Analysis

A measure of potential (AFG analytical GmbH, Leipzig, Germany) was used to determine the Zeta potential values of the drug-loaded samples [26]. The sample was shaken with SGF, SIF, and PBS with pH 1.2, 6.8, and 7.4 at 25 °C for 1 h before measuring.

3. Results and Discussion

3.1. In Situ Synthesis of Composite BC Hydrogels

The extracellular BC synthesis was performed by growing AX in the HS medium under aerobic conditions, with the main process illustrated in Figure 1. After inoculation (day 0), as the bacterial colony growth proceeded, the initial BC began forming. The AX proliferation was promoted by the consumption of oxygen dissolved in the medium [18,27]. On the first inoculation day, the colony was yet to spread to the air-medium interface (Figure 1), with an extremely small amount of cellulose synthesized by the bacteria. As the self-assembly process proceeded, microfibers of 3–6 nm diameter were formed, and these subsequently produced the 40–60 nm BC [28]. Based on our observations, the CSL was found to be a suitable substitute for glucose as a carbon source for growing AX and biosynthesizing BC. Furthermore, the bacterial growth eventually attained the surface of the culture medium on day 4, with the macromolecular compounds (SA or SH) bound to BC produced by the bacteria through hydrogen bonds. Therefore, the AX growth mechanism was unchanged by adding SA or SH, consistent with Wesarg et al. [18]. In synthesizing new layers, the previously synthesized BC layers gradually shifted downward in the medium (day 10), followed by BC synthesis cessation [27].

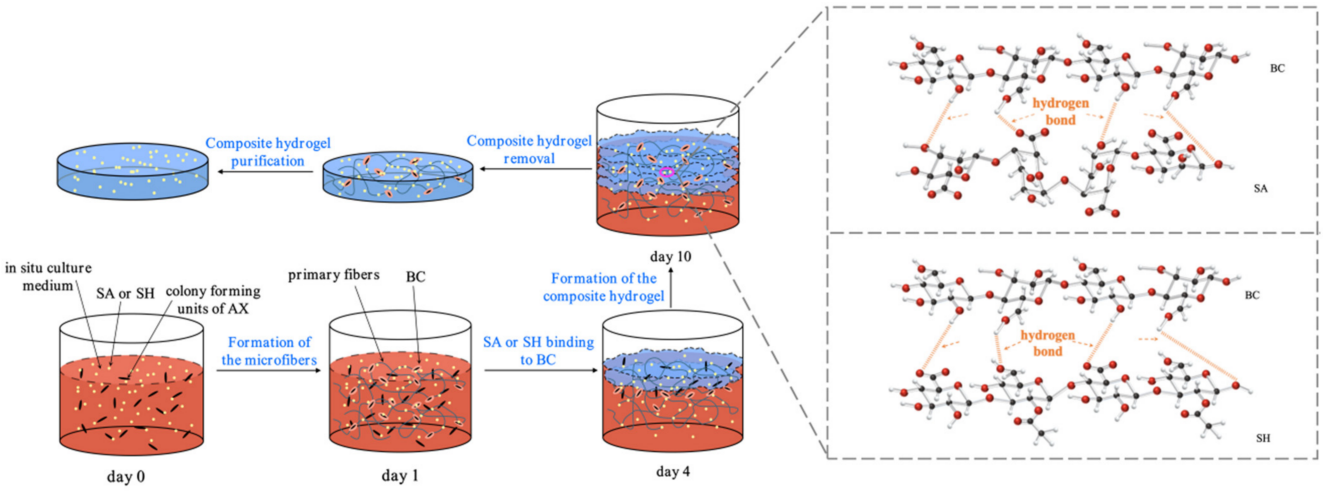


Figure 1. BC formation in the presence of SA/SH.

The synthetic effect of the BC hydrogel was the key factor in the in situ biosynthesis performed in this study. It is vital to evaluate the growth of AX and to ensure the quality of the composite hydrogel. To assess the influence of the macromolecular SA or SH during the biosynthesis, the glucose consumption, bacterial CFUs variation, and the mass weight and yield of the samples were determined. Initially (days 1–2), the adaptation of all the samples occurred in an initial glucose concentration of 20 g/L (Figure 2A), corresponding to a measured initial bacteria colony of 105 CFU/mL (Figure 2B). As the cultivation proceeded, the CSL utilization attained its maximum, with a rapid concentration decrease and exhaustion after 10 days. Between the 2nd and 5th days, most of the aerobic bacteria culture reached the interface, increasing the CFUs to 106/mL (Figure 2B: day 4). Therefore, biosynthesis was reduced due to the lower glucose content and the decreasing number of active cells (Figure 2A,B). The MY of the hydrogels ranged from 14.0% to 41.5% for all the samples (Figure 2C). It can be seen from Figures 2C and 3A, the SA-BC-0.5 and SH-BC-1 exhibited higher MY of 40.0% and 41.5%, respectively, among the seven hydrogel samples. The higher MY indicated that a better synthetic effect and more tridimensional network structure of the composite hydrogel could be obtained. The CSL contained 400 g/L of glucose, which was the carbon source consumed by the AX strain in order to achieve BC synthesis. Faster consumption of the carbon source may be achieved with higher composite efficiency. Additionally, the diffusion of nutrients may have been hindered by the interface,

due to the increasing thickness, thus accelerating the reduction of glucose concentration. This phenomenon is in accordance with that identified in a previous report [18]. Among the hydrogels, those with higher SA or SH dosages in the culture medium yielded higher values and obtained the more tridimensional network structure of the composite hydrogel, indicating higher cross-linking and insolubility. However, the mass weight and yield of the hydrogel were reduced by increasing the quantity of SA to 1.0%. The SA supplement at the dosage of 1.0% in the in situ process causes a remarkable decline in the oxygen transmission rate and thus leads to the inhibition of cell production [22]. The growth of bacteria and the MY of the hydrogel sample were thereby negatively influenced [29]. The optimum production conditions for the composite hydrogels were, therefore, established according to the stated analyses.

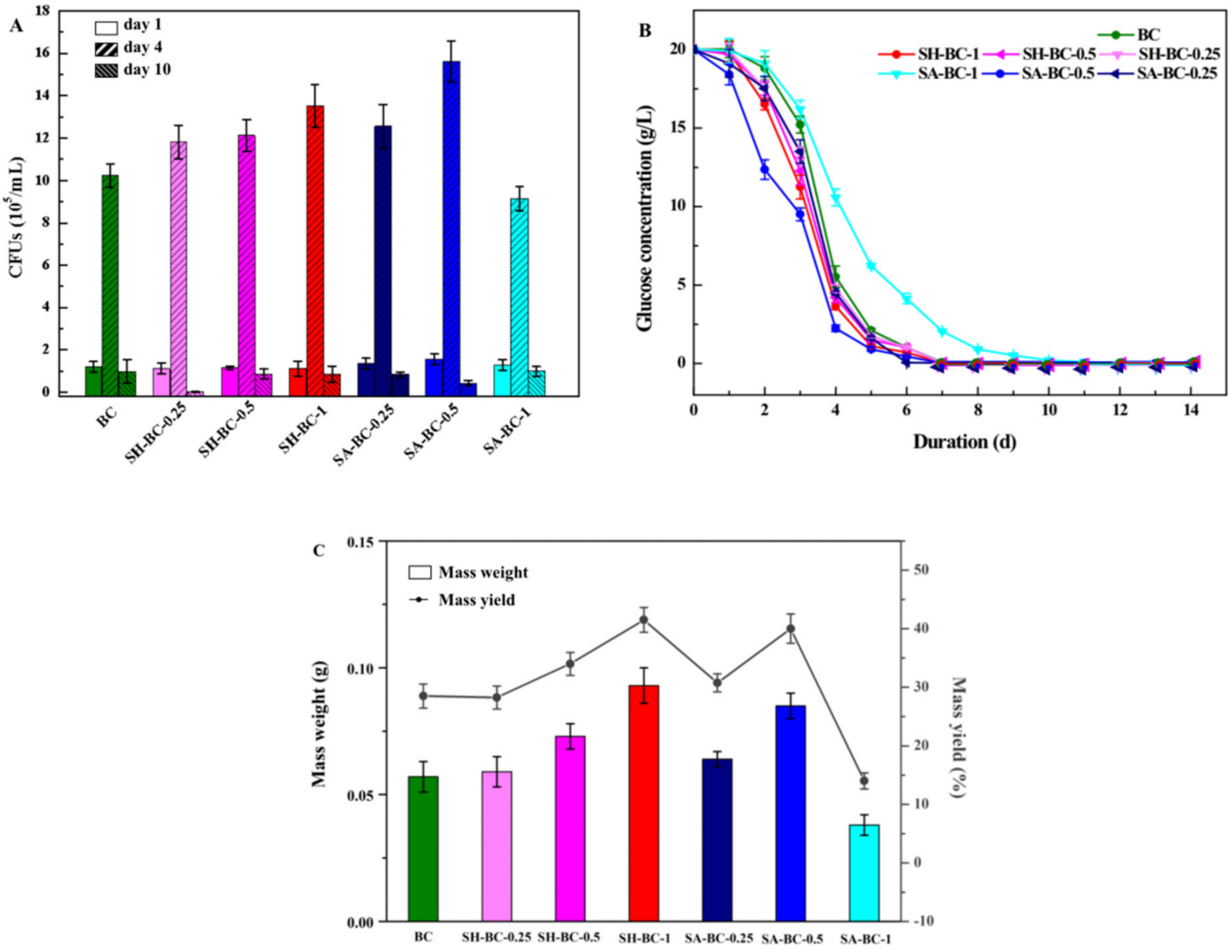


Figure 2. Biosynthesis of the native BC and the composite BC hydrogels (SH-BC-0.25, SH-BC-0.5, SH-BC-1, SA-BC-0.25, SA-BC-0.5, SA-BC-1): CFU number (**A**), glucose consumption (**B**), and mass weight and yield of the cultivation time in days (**C**).

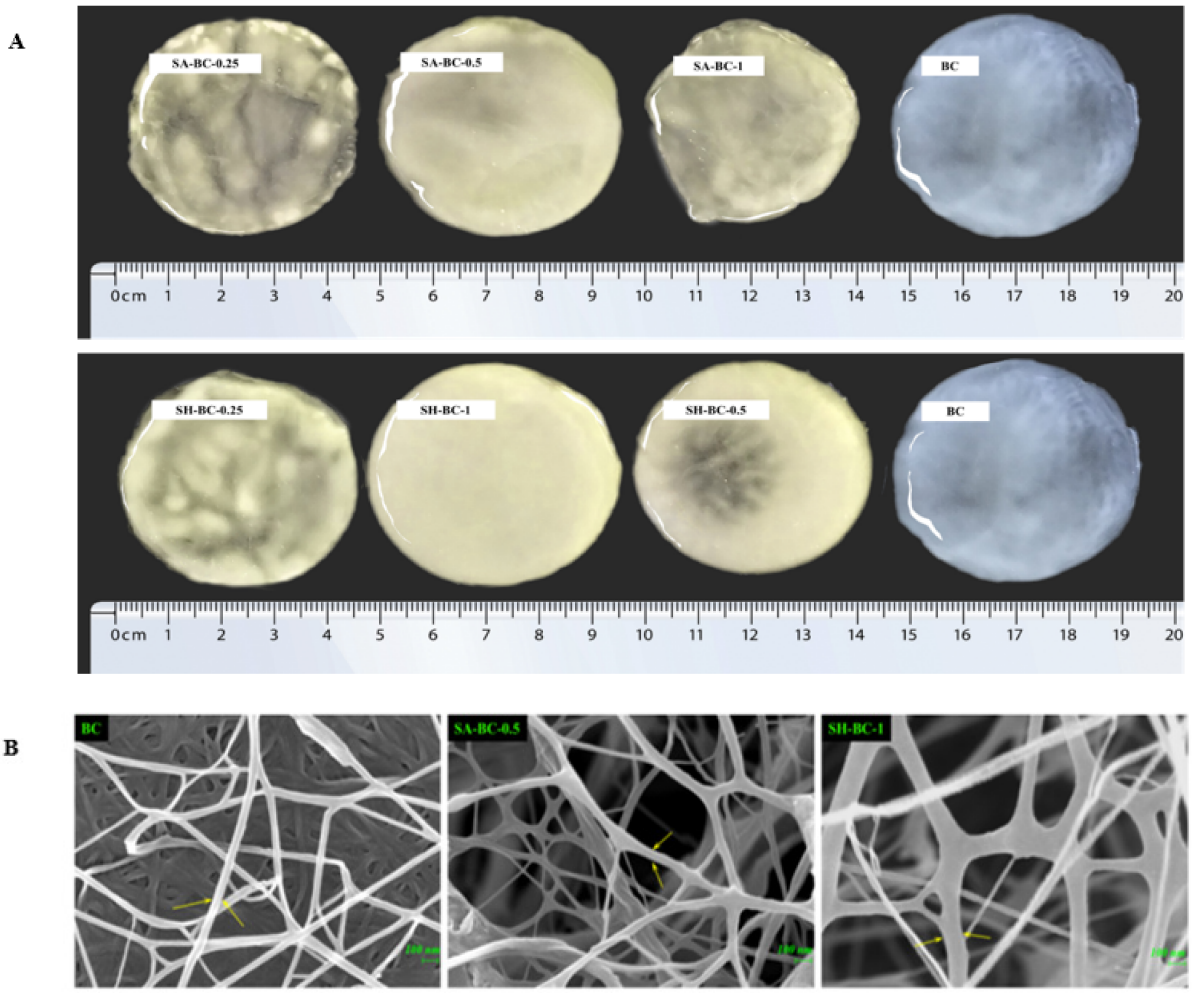


Figure 3. Digital photographs of BC, SA-BC-1, SA-BC-0.5, SA-BC-0.25, SH-BC-1, SH-BC-0.5, and SH-BC-0.25 (**A**); SEM images of BC, SA-BC-0.5, and SH-BC-1 (**B**).

To further evaluate the structure of the hydrogels, optical and micromorphological analyses of the samples were conducted. A typical 3D porous internal network of the composite hydrogel with 0.5% SA or 1% SH, connected to the nanostructure of BC, was displayed (Figure 3B). At a magnification of 50,000×, the transformation of the long, filamentous fibers into interconnected porous structures after the in situ synthesis with SA or SH was evident. Considering the significant difference between the extent of porosity formation and the microfibers' diameter, the microstructural variation of the composite hydrogel network was principally attributed to the in situ synthesis with SA or SH. Compared to SH-BC-1, SA-BC-0.5 contained relatively more sufficient space hierarchy, with a higher possibility for enhancing the sustained-release property of the hydrogel [26]. As the SH dosage increased to 1%, the microfiber diameter became thicker and may potentially contribute to enhancing the mechanical strength of the hydrogel [30]. SEM images of other hydrogels (SH-BC-0.25, SH-BC-0.5, SA-BC-0.25, and SA-BC-1) with decreased nanofiber diameters of 20–35 nm are exhibited in Figure S1 in the Supplementary Materials.

The in situ-derived composite hydrogels exhibited hydrogen bonding of the SA and SH polymers with BC, as shown by the FTIR data shown in Figure 4A. The dispersion of SA or SH in the BC matrix was improved due to the in situ culture mode, forming a net-like structure. This observation was consistent with the XRD and TGA results.

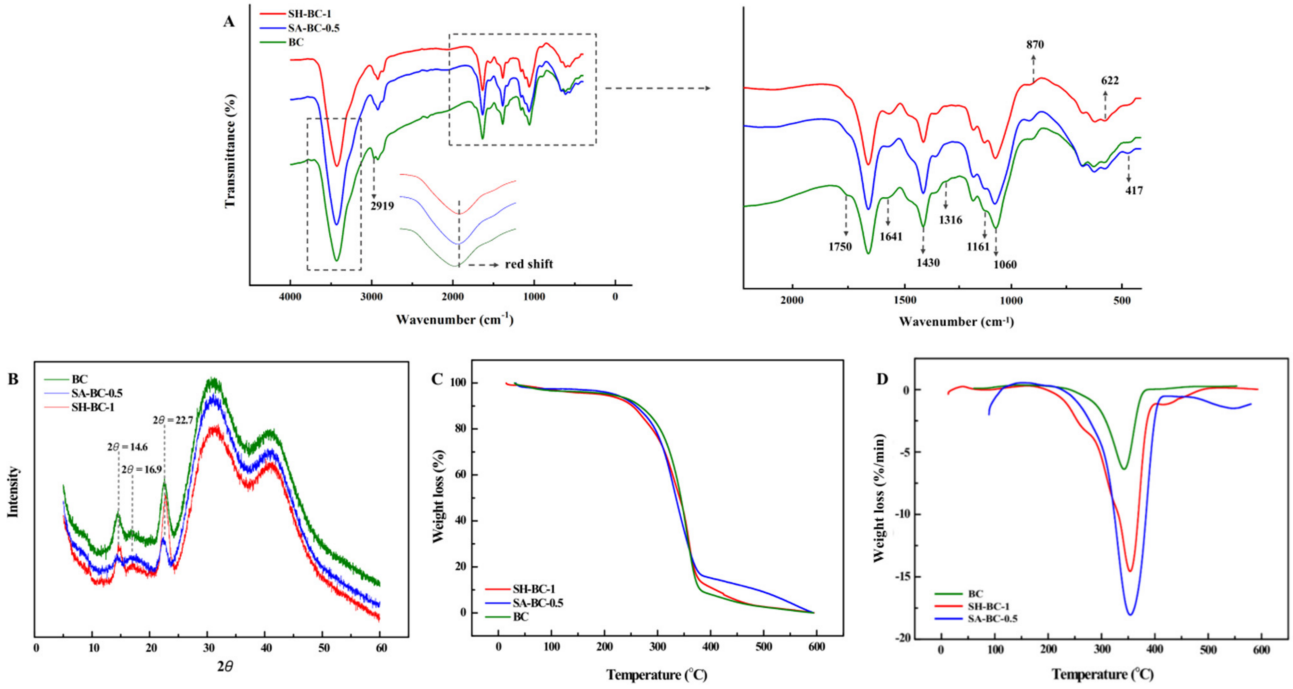


Figure 4. Structural characterization of the native BC and the composite hydrogels (SA-BC-0.5 and SH-BC-1): FTIR (**A**); XRD (**B**); TGA (**C**), and DTG (**D**).

3.2. Structural Characterization

The FTIR spectrum of the native BC in Figure 4A shows that the peak at 1060 cm^{-1} was attributed to the C–O stretching of the primary alcohol. The absorption peaks at 1316 and 1430 cm^{-1} were due to wagging symmetric bending and symmetric bending of CH_2, respectively, and the peaks obtained for the asymmetric stretching of C–O–C and stretching of C–H were at 1161 and 2919 cm^{-1}, respectively [12,31]. The peak at 1750 cm^{-1} was attributed to C=O vibration and the absorption peaks at 622 and 417 cm^{-1} corresponded to –COO– asymmetrical and symmetrical stretching vibrations, respectively [32]. A broad peak at 3400 cm^{-1} was ascribed to O–H stretching and 1641 cm^{-1} was the glucose carbonyl of cellulose [33]. After adding the macromolecular compounds into the medium, a weakened peak appeared at 1750 cm^{-1}, while the peak at 622 cm^{-1} was blunter, and that at 417 cm^{-1} was sharper. The shifting of the peak to a lower wavenumber region emerged at 2919 cm^{-1}. In the SH-BC-1 hydrogel spectrum, the absorption peak at 1161 cm^{-1} was pronounced differently compared with that of the native BC. This illustrates that SH deposition on the BC surface created complex crosslinking during the in situ process. The crosslinking behaviors of SH and BC were also confirmed by the peak at 870 cm^{-1} (N–H bending) [34]. In the SA-BC-0.5 hydrogel spectrum, the intensity difference of the peak at 1641 cm^{-1} demonstrated that binding reactions occurred between SA and BC. Compared with the spectrum of the native BC, the broad and pronounced peaks of a typical red-shift hydrogen bond at 3000–4000 cm^{-1} suggested that the BC could form intermolecular hydrogen bonds with SA or SH [35].

The BC structure contains both a crystalline region and an amorphous region [36]. As seen in Figure 4B, three characteristic peaks appear at 14.6° and 16.9°, and 22.7°, corresponding to the $(1\bar{1}0)$, (110), and (200) planes of the cellulose from the I-β crystal, remained unchanged upon the incorporation of SA or SH in the culture medium [37]. These results revealed that the modification occurred mostly in the amorphous domains [15]. According to the quantified crystal information of each sample (index of crystallinity (CrI), full width at half maximum (FWHM) values, and the crystallite size), SA and SH interfere in the arranged order of the BC chains and thus resulted in the reduced CrI and the weaker diffraction characteristic peaks (Table S2, Supplementary Materials), which is in accordance

with the literature [23]. Based on the reported literature, the characteristic peaks at 14.6° were mainly due to the preferential orientation of the $(1\bar{1}0)$ plane during the dehydration process, which could be inhibited by the existence of a high molecular polymer [23]. The hardness and tensile strength of the material may be increased along with the higher crystallinity, while the larger proportion of amorphous area and the properties of water absorption and chemical reaction would be more satisfactory [38].

The TGA and differential thermal gravimetric (DTG) curves of the in situ-derived hydrogels shown in Figure 4C,D revealed the limited weight loss of the samples from 26–280 °C. The weight loss which occurred in this temperature interval was attributed mainly to the loss of adsorbed water and the water associated with the hydrogen bonds [39]. Due to the stronger hydrogen bond with higher bond energy between BC and SA or SH formed during the in situ synthesis, better thermal stability of the composite hydrogels was observed. In the decomposition of SH-BC-1, the first step was predominantly associated with H_2O release, with the relative stability of the hydrogel below 250 °C. The second step, characterized by the maximum weight loss rate of the decomposed skeleton, fell between 245 and 380 °C, with peaks related to the decomposition of SH appearing at high temperatures [40]. In the third step above 380 °C, further degradation was observed. As shown by the DTG curve, a turning point was present at around 350 °C, indicating the better thermal stability of SH-BC-1 compared to SA-BC-0.5. These results suggested that the cross-linked SH-BC-1 produced a more compact 3D network during the static AX culture. More specifically, additional hydrogen bonds were formed with an increased dosage of the supplemental macromolecule, thus contributing to the composite hydrogel's thermal stability. Moreover, this finding supported that hydrogen bonds could be the source of the differences between SA-BC-1 and SH-BC-0.5 in terms of their mechanical properties [41]. This observation was confirmed by the FTIR and SEM data. Compared to SH-BC-1, the lower initial decomposition temperature of SA-BC-0.5 demonstrated its relatively poorer thermal stability, owing to its higher amorphous cellulose content. These results were also supported by the XRD data. The FTIR, XRD, and thermal characterization of the other hydrogels (SH-BC-0.25, SH-BC-0.5, SA-BC-0.25, and SA-BC-1) were determined and are shown in Figure S2 in the Supplementary Materials.

3.3. Mechanical and Swelling Properties

The tensile strength results for the hydrogel samples are exhibited in Figure 5A. The SA-BC-0.5 and SH-BC-1 hydrogels displayed high tensile strengths of 0.92 and 1.25 MPa at strains of 475% and 574%, respectively. Figure S3 shows that SH-BC-0.25, SH-BC-0.5, SA-BC-0.25, and SA-BC-1 produced testing results of 0.79, 1.07, 0.63, and 0.51 MPa at strains of 452%, 529%, 433%, and 378%, respectively. These tensile strengths were quantitatively evaluated using the striking enhancement, which was attributed to the dispersion of SA or SH particles through the hydrogen bonding interactions. It is worth noting that the increased strain at break of SA-BC-0.5 and SH-BC-1 did not lead to the brittleness of the composite hydrogel with the suitable addition of SA or SH until the amount of SA was increased to 1% (see Figure S3, Supplementary Materials). The low tensile strength seriously affected the mechanical properties of the hydrogel, thus making its degradation feasible. As a result, the limitations of the load-bearing utilization of the hydrogel emerged, leading to its premature dissolution and escape from the target sites of drug delivery systems [42,43]. SH-BC-1 showed better mechanical strength compared with SA-BC-0.5, which implies advantages for different in vivo implantation functional requirements [44], while the produced rigid nanostructure delayed the biodegradation of the scaffold and benefits tissue engineering [35].

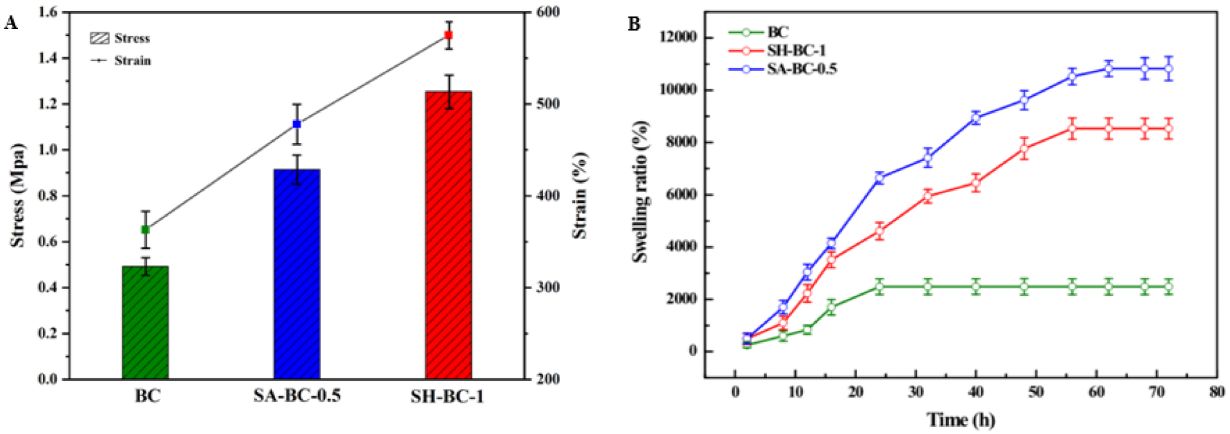


Figure 5. Tensile strength (**A**) and SR (**B**) of the native BC and the composite hydrogels (SA-BC-0.5 and SH-BC-1).

Additionally, the SEM images show that the composite BC hydrogels have a network structure with a porous interior, which indicates that there is great potential for improving their SR. The swelling behaviors of the hydrogels also reflect the absorptive capacity of the hydrogel material to the medium under certain physiological conditions [45]. As a biomaterial, the improved swelling property was accompanied by an increased surface area and enhanced nutrient transport [46]. The SR of the hydrogels after being immersed in a 7.4 pH buffer solution is displayed in Figure 5B. The composite hydrogels of SA-BC-0.5 and SH-BC-1 swelled quickly during the first 16 h. One explanation for this is that contact with water molecules could take place in a relatively short time due to the interconnected pore structure of the composite hydrogels combined with their increased internal specific surface area [47]. It is worth noting that, for the composite hydrogels, the maximum SR of SH-BC-1 at equilibrium was 8603%. The SR of SA-BC was the highest, with a maximum value of 10,831% for the medium with 0.5% SA concentration. The swelling capacity of SH-BC-0.25, SH-BC-0.5, SA-BC-0.25, and SA-BC-1 hydrogels with equilibrium SRs of 7673%, 7976%, 8347%, and 2603%, respectively, are shown in Figure S3 in the Supplementary Materials. When 1% SA was added, the formed linear structure made the hydrogel lose its advantage during its swelling behavior. However, the native BC exhibited a lower SR of 2326% and attained the equilibrium state within 20 h, while the composites of SA-BC-0.5 and SH-BC-1 required approximately 62 h to attain the swelling equilibrium state. This difference in swelling behaviors can be attributed to: (a) the increase in the hydrophilic groups of –COOH in the composite hydrogel chains due to the optimum dose of SA or SH, and (b) the interactions between BC and SA or SH through hydrogen bonds, leading to the denser network of the composite hydrogel (as shown in Figure 3B). The results provide further evidence that the two macromolecules of SA and SH firmly bonded, respectively, in the network structure of the native BC. This good swelling property offers an advantage for biomedical applications. In addition, Yin et al. evaluated the mechanical and swelling properties of the modified BC composite membranes and came to the conclusion that the BC composite membrane with better mechanical properties performed superior swelling capacity, indicating the certain potential for in-depth follow-up research [48].

3.4. In Vitro Drug-Release Studies

The in vitro BSA cumulative release profiles of the hydrogel samples at 37 °C were investigated in SGF, SIF, and PBS at pH values of 1.2, 6.8, and 7.4. The entrapment efficiency (EE) of the native BC, SH-BC-0.25, SH-BC-0.5, SH-BC-1, SA-BC-0.25, SA-BC-0.5, and SA-BC-1 for BSA was 21.33 ± 0.97%, 33.68 ± 0.57%, 34.92 ± 0.83%, 36.75 ± 0.74%, 36.04 ± 0.21%, 40.13 ± 0.82%, and 22.07 ± 0.46%, respectively. Since the denser microstructure with porous and fibrous layers was formed during the in situ synthesis, SA-BC-0.5 or SH-BC-1 likely extended the drug-release time, thereby achieving the aim of sustained release, as

previously indicated. A declining trend was observed in the cumulative release for the SA-BC and SH-BC hydrogel samples as the pH decreased from 7.4 to 1.2 (Figure 6), and the maximum cumulative percentage release of the loaded BSA varied. For SH-BC-1, the maximum cumulative percentage release value was 89.93% at pH 7.4, 77.81% at pH 6.8, and 73.44% at pH 1.2. For SA-BC-0.5, the maximum cumulative percentage release value was 92.55% at pH 7.4, 82.12% at pH 6.8, and 75.02% at pH 1.2. However, there was no discernible distinction for the native BC. According to the SEM images and the swelling property results, the native BC material lacked a uniform network structure. The differences in cumulative percentage release of the loaded BSA in the composite hydrogels can be attributed to the release conditions with different pH values. As can be seen in Figure S4 in the Supplementary Materials, for SA-BC-0.25, the maximum cumulative percentage release value was 84.12% at pH 7.4, 73.40% at pH 6.8, and 69.10% at pH 1.2, while that of SH-BC-0.5 was 83.24% at pH 7.4, 76.55% at pH 6.8, and 70.58% at pH 1.2. SA-BC-1 lacked a porous network structure and the drug release for BSA was limited. Under subalkaline conditions (pH 7.4), the $–COO^-$ groups of the composite hydrogel bound to $–NH_3^+$ of BSA. The better release behaviors of the composite hydrogels may be because of the synergistic effect of electrostatic forces and molecular chain stretching [49]. The –COO– groups were transformed to –COOH from pH 1.2 to pH 6.8, which weakened the combined intensity between the hydrogel and BSA. These findings suggest that, due to the better-released effect of BSA at the subalkaline pH of 7.4, both SA-BC-0.5 and SH-BC-1 exhibited tremendous potential as a controlled protein-based drug-delivery system. Consistent with the data obtained from the swelling studies, SA-BC-0.5 resulted in the highest cumulative percentage release among the seven hydrogel samples. The simulations also displayed that the addition of SA had exclusive advantages in the in vitro drug-release system. In addition, the synthesized SH-BC-1 with improved mechanical and thermal stabilities offered an opportunity for the delayed biodegradation of the biomedical material. Thus, SA-BC-0.5 and SH-BC-1 composite hydrogels are considered excellent candidates for controlled drug delivery systems.

In Figure 6D, SA-BC-0.5 and SH-BC-1 composite hydrogel samples displayed distinct zeta potentials in the buffer solutions at different pH values. Although the SA-BC-0.5 sample showed a high absolute zeta potential of 73.9 mV in the 7.4 pH buffer solution, the potentials for SA-BC-0.5 and SH-BC-1, and other hydrogel samples (see Figure S4), decreased at pH values of 1.2 and 6.8. This decline is attributed to the dissociation of -COOH groups at the alkaline pH value and a decreased ionization at the acidic pH values [49].

The mechanism of this composite hydrogel is that BC was firstly biosynthesized by the AX strain in the cell and subsequently transported from the cell [50]. Meanwhile, the synthesized BC was crosslinked with the extracellular macromolecule (i.e., SA and SH) through the hydrogen bond to form composite biomacromolecules with a 3D spatial structure, namely hydrogels. BC itself is a type of hydrogel, but it possesses relatively poor properties. After being composed with SA or SH, the composite BC hydrogel with a higher SR and sustained release ability was formed. Different results of the native BC and the six composite hydrogels were found due to the growth of the bacterial strain (glucose consumption and CFUs numbers), the yield of the fermentative product (mass weight and yield), and the structural characterization and important characteristics (tensile strength, swelling capacity, and drug release property for BSA). The experimental results of the seven hydrogel samples strongly suggest that the structure of the composite hydrogel with a higher MY would be more tridimensional to uncover the potentiality of properties with broad application prospects (e.g., biomedicine). The results illustrate that SH-BC-1 has superior mechanical properties compared to SA-BC. SA-BC-0.5 showed high swelling capacity performance and an effective sustained-release property.

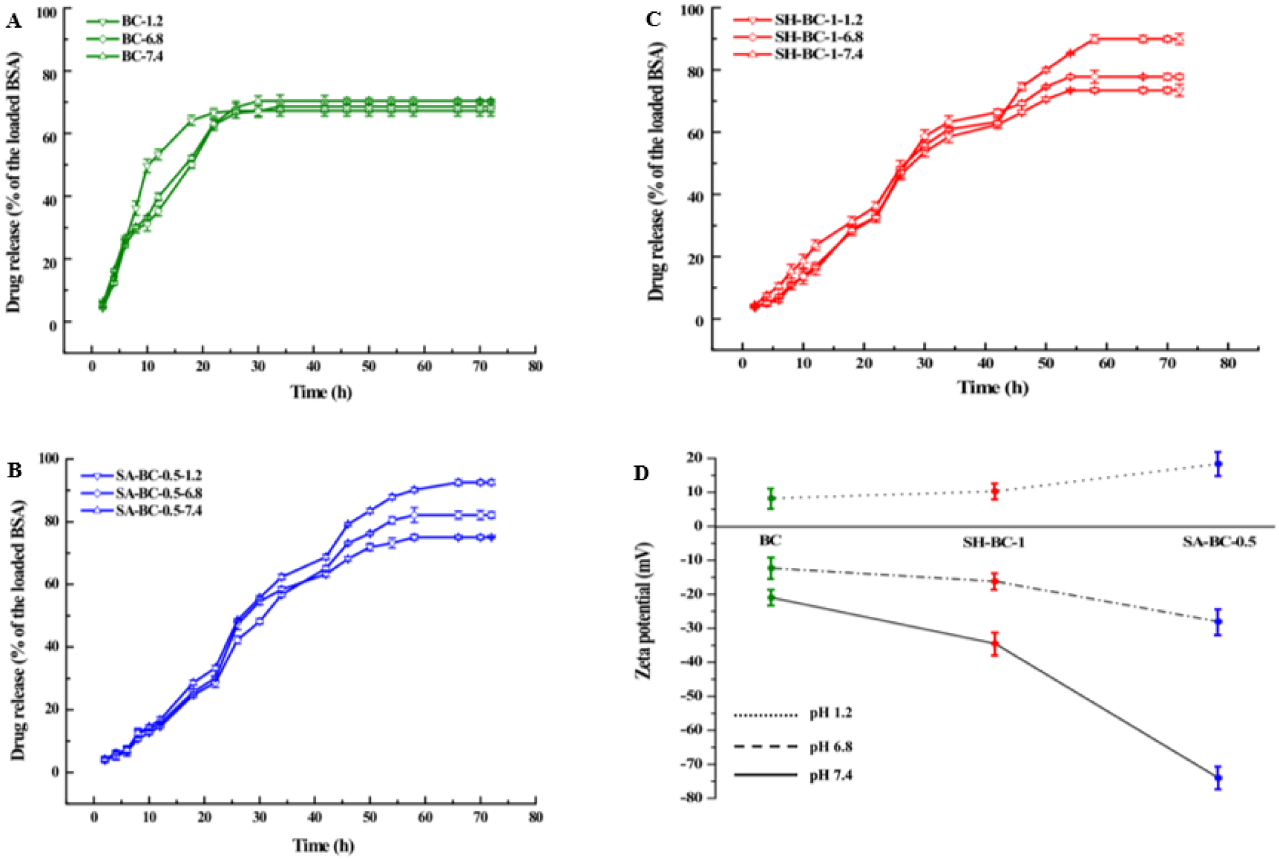


Figure 6. Profiles of the in vitro drug release efficiency (**A**) BC, (**B**) SA-BC-0.5, (**C**) SH-BC-1, and (**D**) zeta potential.

The pH-sensitive drug-release behaviors of the hydrogel samples attributed to the change of molecular form are shown in Figure 7. Under acidic conditions (pH 1.2 and 6.8), the -COO- groups had a great binding ability with H^+, and the hydrophilicity of SA or SH was reduced with the ionization decrease. Under these conditions, the molecule chains were inclined to shrink. Conversely, the hydrophilicity increased in the subalkaline environment (pH 7.4), inducing the stretching of the molecular chains. The hydrogen bonding interaction also weakened due to anionic electrostatic repulsion [49]. Therefore, SA-BC-0.5 and SH-BC-1 exhibited apparent pH sensitivity. These findings demonstrate that SA-BC-0.5 hydrogel offers great potential for controlled protein-based drug-delivery systems, especially in subalkaline environments.

As a basic detection method, cytotoxicity provides high reliability to assess the biocompatibility of a material [51]. In this study, the cytotoxicities of BC, SH-BC-0.25, SH-BC-0.5, SH-BC-1, SA-BC-0.25, SA-BC-0.5, and SA-BC-1 samples toward cultured Hela cells determined by the MTT assay are shown in Figure S5. The results indicated that no apparent differences in the cell viability of cultured Hela cells were observed in the presence of the seven hydrogel samples or the control; the observed enhanced cell growth provided further evidence that SA and SH are biodegradable polymers with negligible cell cytotoxicity [52]. Therefore, the produced composite hydrogels are suitable for drug delivery systems.

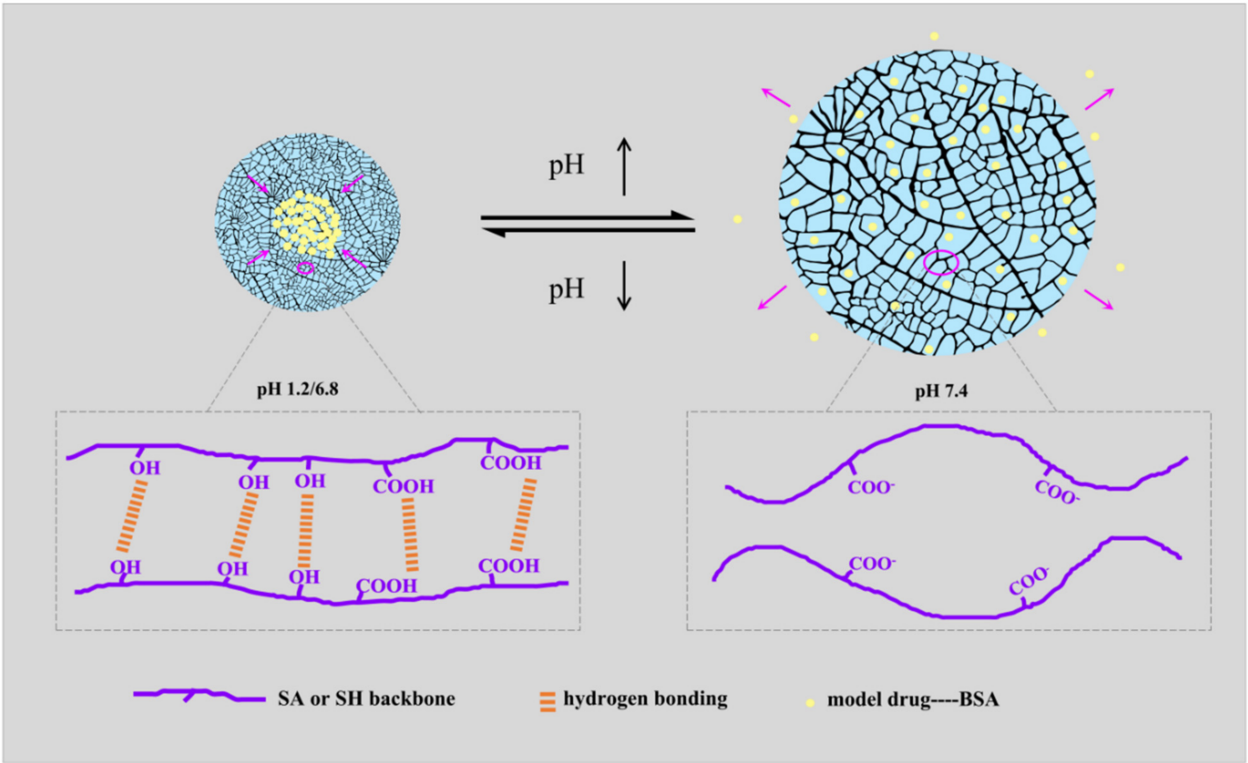


Figure 7. Schematic mechanism of pH-responsive release behavior of the composite hydrogels.

4. Conclusions

SA-BC and SH-BC composite hydrogel nanostructures were fabricated via an in situ modification strategy. The nutritional properties of CSL could meet the need for carbon sources for BC. SA or SH and were distributed across the resulting composite hydrogel network through hydrogen bonding with BC. In comparison with the native BC, SH-BC displayed better mechanical properties at an appropriate SH concentration and SH-BC-1 had superior mechanical properties compared to SA-BC, indicating that the desired porous structure was produced without sacrificing mechanical strength stability. The in vitro cumulative drug-release results suggest that the composite BC hydrogels were pH-sensitive owing to -COOH generation from the –COO– groups and stronger hydrogen bonding interaction in the acidic environments. By combining the morphology characterization and an extraordinary swelling ratio of %, a better-sustained release performance was produced by the more abundant and multi-layered SA-BC network containing 0.5% SA. No obvious cytotoxicity for the composite hydrogels after 2 days indicates good cytocompatibility. Considering the stated advantages, this study confirms that composite BC hydrogels could be fabricated through an in situ microbial synthesis system with CSL substituting for glucose as the carbon source in the medium. These findings offer prospects for the transformation of polysaccharides to biocompatible and biodegradable materials, with the potential to replace petroleum-based composites in many applications on the principle of "sustainable development".

Supplementary Materials: The following supporting information can be downloaded at: https://www.mdpi.com/article/10.3390/su142114277/s1, Materials; Method of CSL perpetration; In vitro cytotoxicity assay; SA and SH contents during the in situ process; Table S1: The contents of SA and SH during the in situ microbial synthesis system; Table S2: Structural parameters calculated from XRD data; Figure S1: SEM images of SH-BC-0.25, SH-BC-0.5, SA-BC-0.25, and SA-BC-1; Figure S2: Structural characterization of SH-BC-0.25, SH-BC-0.5, SA-BC-0.25, and SA-BC-1: FTIR (A), XRD (B), TGA (C) and DTG (D); Figure S3: Tensile strength (A) and SR (B) of SH-BC-0.25, SH-BC-0.5, SA-BC-0.25, and SA-BC-1; Figure S4: Profiles of the in vitro drug release efficiency (A) SH-BC-0.25, (B) SH-BC-0.5,

(C) SA-BC-0.25, (D) SA-BC-1 and (E) zeta potential; Figure S5: The cytotoxicity measure of BC, SH-BC-0.25, SH-BC-0.5, SH-BC-1, SA-BC-0.25, SA-BC-0.5, and SA-BC-1. Refs. [5,15,23,34,35,37,47,49,53–56] are citied in supplementary materials.

Author Contributions: Data curation, L.J.; Funding acquisition, J.J.; Investigation, W.X.; Methodology, L.Z.; Project administration, L.J.; Supervision, J.J.; Validation, W.X. and L.Z.; Writing–original draft, L.J. All authors have read and agreed to the published version of the manuscript.

Funding: This work was supported by the National Natural Science Foundation of China (No. 32001339) and the Fundamental Research Funds for the Central Universities (BLX202130).

Data Availability Statement: E-supplementary data of this work can be found in the online version of the paper.

Conflicts of Interest: The authors declare no competing financial interest.

Abbreviations

BC: bacterial cellulose; SA, sodium alginate; SH, sodium hyaluronate; AX, *Acetobacter xylinum*; CR, cassava residue; CSL, cassava residue saccharification liquid; BSA, bovine serum albumin; HS, Hestrin–Schramm; MS, mass yield; CFUs, colony forming units; SR, swelling ratio; SGF, simulated gastric fluid; SIF, simulated intestinal fluid; EE, entrapment efficiency; FTIR, Fourier-transform infrared; XRD, X-ray diffraction; SEM, scanning electron microscopy; TGA, thermogravimetric analysis; DTG, differential thermal gravimetric.

References

1. Revin, V.V.; Pestov, N.A.; Shchankin, M.V.; Mishkin, V.P.; Platonov, V.I.; Uglanov, D.A. A Study of the Physical and Mechanical Properties of Aerogels Obtained from Bacterial Cellulose. *Biomacromolecules* **2019**, *20*, 1401–1411. [CrossRef] [PubMed]
2. Baksi, S.; Ball, A.K.; Sarkar, U.; Banerjee, D.; Wentzel, A.; Preisig, H.A.; Kuniyal, J.C.; Birgen, C.; Saha, S.; Wittgens, B.; et al. Efficacy of a novel sequential enzymatic hydrolysis of lignocellulosic biomass and inhibition characteristics of monosugars. *Int. J. Biol. Macromol.* **2019**, *129*, 634–644. [CrossRef] [PubMed]
3. Azlan, N.S.M.; Yap, C.L.; Gan, S.; Rahman, M.B.A. Recent advances in the conversion of lignocellulosic biomass and its degraded products to levulinic acid: A synergy of Brønsted-Lowry acid and Lewis acid. *Ind. Crop. Prod.* **2022**, *181*, 114778. [CrossRef]
4. Rajendran, K.; Drielak, E.; Varma, V.S.; Muthusamy, S.; Kumar, G. Updates on the pretreatment of lignocellulosic feedstocks for bioenergy production—A review. *Biomass-Convers. Biorefin.* **2017**, *8*, 471–483. [CrossRef]
5. Ji, L.; Zheng, T.; Zhao, P.; Zhang, W.; Jiang, J. Ethanol production from a biomass mixture of furfural residues with green liquor-peroxide saccarified cassava liquid. *BMC Biotechnol.* **2016**, *16*, 1–11. [CrossRef] [PubMed]
6. Arevalo-Gallegos, A.; Ahmad, Z.; Asgher, M.; Parra-Saldivar, R.; Iqbal, H.M. Lignocellulose: A sustainable material to produce value-added products with a zero waste approach—A review. *Int. J. Biol. Macromol.* **2017**, *99*, 308–318. [CrossRef] [PubMed]
7. Wu, Z.; Chen, S.; Wu, R.; Sheng, N.; Zhang, M.; Ji, P.; Wang, H. Top-down peeling bacterial cellulose to high strength ultrathin films and multifunctional fibers. *Chem. Eng. J.* **2019**, *391*, 123527. [CrossRef]
8. Rahman, M.M.; Netravali, A.N. Aligned Bacterial Cellulose Arrays as "Green" Nanofibers for Composite Materials. *ACS Macro Lett.* **2016**, *5*, 1070–1074. [CrossRef]
9. Tang, S.; Chi, K.; Xu, H.; Yong, Q.; Yang, J.; Catchmark, J.M. A covalently cross-linked hyaluronic acid/bacterial cellulose composite hydrogel for potential biological applications. *Carbohydr. Polym.* **2020**, *252*, 117123. [CrossRef]
10. Liu, W.; Du, H.; Zhang, M.; Liu, K.; Liu, H.; Xie, H.; Zhang, X.; Si, C. Bacterial Cellulose-Based Composite Scaffolds for Biomedical Applications: A Review. *ACS Sustain. Chem. Eng.* **2020**, *8*, 7536–7562. [CrossRef]
11. Gorgieva, S.; Hribernik, S. Microstructured and Degradable Bacterial Cellulose–Gelatin Composite Membranes: Mineralization Aspects and Biomedical Relevance. *Nanomaterials* **2019**, *9*, 303. [CrossRef] [PubMed]
12. Huang, J.; Deng, Y.; Ren, J.; Chen, G.; Wang, G.; Wang, F.; Wu, X. Novel in situ forming hydrogel based on xanthan and chitosan re-gelifying in liquids for local drug delivery. *Carbohydr. Polym.* **2018**, *186*, 54–63. [CrossRef] [PubMed]
13. Yang, J.; Lv, X.; Chen, S.; Li, Z.; Feng, C.; Wang, H.; Xu, Y. In situ fabrication of a microporous bacterial cellulose/potato starch composite scaffold with enhanced cell compatibility. *Cellulose* **2014**, *21*, 1823–1835. [CrossRef]
14. Mohamad, N.; Amin, M.C.I.M.; Pandey, M.; Ahmad, N.; Rajab, N.F. Bacterial cellulose/acrylic acid hydrogel synthesized via electron beam irradiation: Accelerated burn wound healing in an animal model. *Carbohydr. Polym.* **2014**, *114*, 312–320. [CrossRef]
15. Gao, M.; Li, J.; Bao, Z.; Hu, M.; Nian, R.; Feng, D.; An, D.; Li, X.; Xian, M.; Zhang, H. A natural in situ fabrication method of functional bacterial cellulose using a microorganism. *Nat. Commun.* **2019**, *10*, 1–10. [CrossRef] [PubMed]

16. Urbina, L.; Eceiza, A.; Gabilondo, N.; Corcuera, M.; Retegi, A. Tailoring the in situ conformation of bacterial cellulose-graphene oxide spherical nanocarriers. *Int. J. Biol. Macromol.* **2020**, *163*, 1249–1260. [CrossRef]
17. Ji, L.; Zhang, F.; Zhu, L.; Jiang, J. An in-situ fabrication of bamboo bacterial cellulose/sodium alginate nanocomposite hydrogels as carrier materials for controlled protein drug delivery. *Int. J. Biol. Macromol.* **2021**, *170*, 459–468. [CrossRef]
18. Wesarg, F.; Schlott, F.; Grabow, J.; Kurland, H.-D.; Heßler, N.; Kralisch, D.; Müller, F.A. In Situ Synthesis of Photocatalytically Active Hybrids Consisting of Bacterial Nanocellulose and Anatase Nanoparticles. *Langmuir* **2012**, *28*, 13518–13525. [CrossRef]
19. Chi, K.; Catchmark, J.M. The influences of added polysaccharides on the properties of bacterial crystalline nanocellulose. *Nanoscale* **2017**, *9*, 15144–15158. [CrossRef]
20. Hernández-González, A.C.; Téllez-Jurado, L.; Rodríguez-Lorenzo, L.M. Alginate hydrogels for bone tissue engineering, from injectables to bioprinting: A review. *Carbohydr. Polym.* **2019**, *229*, 115514. [CrossRef]
21. Das, D.; Pham, T.T.H.; Noh, I. Characterizations of hyaluronate-based terpolymeric hydrogel synthesized via free radical polymerization mechanism for biomedical applications. *Colloids Surf. B Biointerfaces* **2018**, *170*, 64–75. [CrossRef] [PubMed]
22. Kanjanamosit, N.; Muangnapoh, C.; Phisalaphong, M. Biosynthesis and characterization of bacteria cellulose-alginate film. *J. Appl. Polym. Sci.* **2009**, *115*, 1581–1588. [CrossRef]
23. Kim, J.H.; Park, S.; Kim, H.; Kim, H.J.; Yang, Y.-H.; Kim, Y.H.; Jung, S.-K.; Kan, E.; Lee, S.H. Alginate/bacterial cellulose nanocomposite beads prepared using Gluconacetobacter xylinus and their application in lipase immobilization. *Carbohydr. Polym.* **2017**, *157*, 137–145. [CrossRef] [PubMed]
24. Yang, Y.; Wang, X.; Yang, F.; Wang, L.; Wu, D. Highly Elastic and Ultratough Hybrid Ionic-Covalent Hydrogels with Tunable Structures and Mechanics. *Adv. Mater.* **2018**, *30*, e1707071. [CrossRef]
25. Fredua-Agyeman, M.; Gaisford, S. Comparative survival of commercial probiotic formulations: Tests in biorelevant gastric fluids and real-time measurements using microcalorimetry. *Benef. Microbes* **2015**, *6*, 141–151. [CrossRef]
26. Amin, M.C.I.M.; Ahmad, N.; Halib, N.; Ahmad, I. Synthesis and characterization of thermo- and pH-responsive bacterial cellulose/acrylic acid hydrogels for drug delivery. *Carbohydr. Polym.* **2012**, *88*, 465–473. [CrossRef]
27. Klemm, D.; Schumann, D.; Udhardt, U.; Marsch, S. Bacterial synthesized cellulose—Artificial blood vessels for microsurgery. *Prog. Polym. Sci.* **2001**, *26*, 1561–1603. [CrossRef]
28. Koizumi, S.; Yue, Z.; Tomita, Y.; Kondo, T.; Iwase, H.; Yamaguchi, D.; Hashimoto, T. Bacterium organizes hierarchical amorphous structure in microbial cellulose. *Eur. Phys. J. E* **2008**, *26*, 137–142. [CrossRef]
29. Zhou, L.L.; Sun, D.P.; Hu, L.Y.; Li, Y.W.; Yang, J.Z. Effect of addition of sodium alginate on bacterial cellulose production by Acetobacter xylinum. *J. Ind. Microbiol. Biotechnol.* **2007**, *34*, 483–489. [CrossRef]
30. Pan, X.; Wang, Q.; Ning, D.; Dai, L.; Liu, K.; Ni, Y.; Chen, L.; Huang, L. Ultraflexible Self-Healing Guar Gum-Glycerol Hydrogel with Injectable, Antifreeze, and Strain-Sensitive Properties. *ACS Biomater. Sci. Eng.* **2018**, *4*, 3397–3404. [CrossRef]
31. Si, H.; Luo, H.; Xiong, G.; Yang, Z.; Raman, S.R.; Guo, R.; Wan, Y. One-Step In Situ Biosynthesis of Graphene Oxide-Bacterial Cellulose Nanocomposite Hydrogels. *Macromol. Rapid Commun.* **2014**, *35*, 1706–1711. [CrossRef] [PubMed]
32. Islam, S.; Karim, M.R. Fabrication and characterization of poly(vinyl alcohol)/alginate blend nanofibers by electrospinning method. *Colloids Surf. A Physicochem. Eng. Asp.* **2010**, *366*, 135–140. [CrossRef]
33. Jia, Y.; Wang, X.; Huo, M.; Zhai, X.; Li, F.; Zhong, C. Preparation and characterization of a novel bacterial cellulose/chitosan bio-hydrogel. *Nanomater. Nanotechnol.* **2017**, *7*, 1–8. [CrossRef]
34. Franca, C.A.; Etcheverry, S.B.; Diez, R.P.; Williams, P.A.M. Irbesartan: FTIR and Raman spectra. Density functional study on vibrational and NMR spectra. *J. Raman Spectrosc.* **2009**, *40*, 1296–1300. [CrossRef]
35. Yan, H.; Huang, D.; Chen, X.; Liu, H.; Feng, Y.; Zhao, Z.; Dai, Z.; Zhang, X.; Lin, Q. A novel and homogeneous scaffold material: Preparation and evaluation of alginate/bacterial cellulose nanocrystals/collagen composite hydrogel for tissue engineering. *Polym. Bull.* **2017**, *75*, 985–1000. [CrossRef]
36. Barros, S.C.; Da Silva, A.A.; Costa, D.B.; Costa, C.M.; Lanceros-Mendez, S.; Maciavello, M.N.T.; Ribelles, J.L.G.; Sentanin, F.; Pawlicka, A.; Silva, M.M. Thermal–mechanical behaviour of chitosan–cellulose derivative thermoreversible hydrogel films. *Cellulose* **2015**, *22*, 1911–1929. [CrossRef]
37. Gaspar, D.; Fernandes, S.; De Oliveira, A.G.; Fernandes, J.G.; Grey, P.; Pontes, R.V.; Pereira, L.; Martins, R.; Godinho, M.H.; Fortunato, E. Nanocrystalline cellulose applied simultaneously as the gate dielectric and the substrate in flexible field effect transistors. *Nanotechnology* **2014**, *25*, 094008. [CrossRef]
38. Tazi, M.; Erchiqui, F.; Kaddami, H. Influence of SOFTWOOD-fillers content on the biodegradability and morphological properties of WOOD-polyethylene composites. *Polym. Compos.* **2016**, *39*, 29–37. [CrossRef]
39. Pajchel, L.; Kolodziejski, W. Solid-state MAS NMR, TEM, and TGA studies of structural hydroxyl groups and water in nanocrystalline apatites prepared by dry milling. *J. Nanopart. Res.* **2013**, *15*, 1–15. [CrossRef]
40. Ma, R.; Epand, R.; Zhitomirsky, I. Electrodeposition of hyaluronic acid and hyaluronic acid–bovine serum albumin films from aqueous solutions. *Colloids Surf. B Biointerfaces* **2010**, *77*, 279–285. [CrossRef]
41. Rosen-Kligvasser, J.; Davidovich-Pinhas, M. The role of hydrogen bonds in TAG derivative-based oleogel structure and properties. *Food Chem.* **2020**, *334*, 127585. [CrossRef] [PubMed]
42. Mandal, B.B.; Kapoor, S.; Kundu, S.C. Silk fibroin/polyacrylamide semi-interpenetrating network hydrogels for controlled drug release. *Biomaterials* **2009**, *30*, 2826–2836. [CrossRef] [PubMed]
43. Hoare, T.R.; Kohane, D.S. Hydrogels in drug delivery: Progress and challenges. *Polymer* **2008**, *49*, 1993–2007. [CrossRef]

44. Hong, Y.; Huber, A.; Takanari, K.; Amoroso, N.; Hashizume, R.; Badylak, S.; Wagner, W.R. Mechanical properties and in vivo behavior of a biodegradable synthetic polymer microfiber–extracellular matrix hydrogel biohybrid scaffold. *Biomaterials* **2011**, *32*, 3387–3394. [CrossRef]
45. Sowjanya, J.; Singh, J.; Mohita, T.; Sarvanan, S.; Moorthi, A.; Srinivasan, N.; Selvamurugan, N. Biocomposite scaffolds containing chitosan/alginate/nano-silica for bone tissue engineering. *Colloids Surf. B Biointerfaces* **2013**, *109*, 294–300. [CrossRef]
46. Zonatto, F.; Muniz, E.C.; Tambourgi, E.B.; Paulino, A.T. Adsorption and controlled release of potassium, phosphate and ammonia from modified Arabic gum-based hydrogel. *Int. J. Biol. Macromol.* **2017**, *105*, 363–369. [CrossRef]
47. Hu, X.; Feng, L.; Xie, A.; Wei, W.; Wang, S.; Zhang, J.; Dong, W. Synthesis and characterization of a novel hydrogel: Salecan/polyacrylamide semi-IPN hydrogel with a desirable pore structure. *J. Mater. Chem. B* **2014**, *2*, 3646–3658. [CrossRef]
48. Yin, N.; Du, R.; Zhao, F.; Han, Y.; Zhou, Z. Characterization of antibacterial bacterial cellulose composite membranes modified with chitosan or chitooligosaccharide. *Carbohydr. Polym.* **2020**, *229*, 115520. [CrossRef]
49. Ullah, H.; Wahid, F.; Santos, H.A.; Khan, T. Advances in biomedical and pharmaceutical applications of functional bacterial cellulose-based nanocomposites. *Carbohydr. Polym.* **2016**, *150*, 330–352. [CrossRef]
50. Sakairi, N.; Suzuki, S.; Ueno, K.; Han, S.-M.; Nishi, N.; Tokura, S. Biosynthesis of hetero-polysaccharides by Acetobacter xylinum—Synthesis and characterization of metal-ion adsorptive properties of partially carboxymethylated cellulose. *Carbohydr. Polym.* **1998**, *37*, 409–414. [CrossRef]
51. Wang, D.; Wang, L.; Lou, Z.; Zheng, Y.; Wang, K.; Zhao, L.; Han, W.; Jiang, K.; Shen, G. Biomimetic, biocompatible and robust silk Fibroin-MXene film with stable 3D cross-link structure for flexible pressure sensors. *Nano Energy* **2020**, *78*, 105252. [CrossRef]
52. Balakrishnan, B.; Mohanty, M.; Umashankar, P.; Jayakrishnan, A. Evaluation of an in situ forming hydrogel wound dressing based on oxidized alginate and gelatin. *Biomaterials* **2005**, *26*, 6335–6342. [CrossRef] [PubMed]
53. Cui, N.; Qian, J.; Liu, T.; Zhao, N.; Wang, H. Hyaluronic acid hydrogel scaffolds with a triple degradation behavior for bone tissue engineering. *Carbohydr. Polym.* **2015**, *126*, 192–198. [CrossRef] [PubMed]
54. Kim, C.; Jeong, D.; Kim, S.; Kim, Y.; Jung, S. Cyclodextrin functionalized agarose gel with low gelling temperature for controlled drug delivery systems. *Carbohydr. Polym.* **2019**, *222*, 115011. [CrossRef] [PubMed]
55. Xu, L.M.; Chen, L.; Dong, Z.; Wang, J.; Wang, Z.J.; Shao, A.L. In vivo toxicity and in vitro cytotoxicity of silver nanoparticle based-hydrogel in reproductive organs of rabbit and Hela sells. *Chin. J. Pharm. Anal.* **2012**, *32*, 194–201.
56. Yuan, M.; Bi, B.; Huang, J.; Zhuo, R.; Jiang, X. Thermosensitive and photocrosslinkable hydroxypropyl chitin-based hydrogels for biomedical applications. *Carbohydr. Polym.* **2018**, *192*, 10–18. [CrossRef]